

Lamina-Specific Distribution of Synaptopodin, an Actin-Associated Molecule Essential for the Spine Apparatus, in Identified Principal Cell Dendrites of the Mouse Hippocampus

CARLOS BAS ORTH,¹ ANDREAS VLACHOS,¹ DOMENICO DEL TURCO,¹
GUIDO J. BURBACH,¹ CAROLA A. HAAS,² PETER MUNDEL,³ GUOPING FENG,⁴
MICHAEL FROTSCHER,² AND THOMAS DELLER^{1*}

¹Institute of Clinical Neuroanatomy, J. W. Goethe University,
D-60590 Frankfurt/Main, Germany

²Institute of Anatomy and Cell Biology, University of Freiburg, D-79001 Freiburg, Germany

³Division of Nephrology, Albert Einstein College of Medicine, Bronx, New York 10461

⁴Department of Neurobiology, Duke University Medical Center,
Durham, North Carolina 27710

ABSTRACT

Synaptopodin is an actin-associated molecule found in a subset of telencephalic spines. It is an essential component of the spine apparatus, a Ca²⁺-storing organelle and has been implicated in synaptic plasticity (Deller et al. [2003] Proc Natl Acad Sci U S A 100:10494–10499). In the rodent hippocampus, Synaptopodin is distributed in a characteristic region- and lamina-specific manner. To learn more about the cellular basis underlying this distribution, the regional, laminar, and cellular localization of Synaptopodin and its mRNA were analyzed in mouse hippocampus. First, Synaptopodin puncta densities were quantified after immunofluorescent labeling using confocal microscopy. Second, the dendritic distribution of Synaptopodin-positive puncta was studied using three-dimensional confocal reconstructions of Synaptopodin-immunostained and enhanced green fluorescence protein (EGFP)-labeled principal neurons. Synaptopodin puncta located within dendrites of principal neurons were primarily found in spines (>95%). Analysis of dendritic segments located in different layers revealed lamina-specific differences in the percentage of Synaptopodin-positive spines. Densities ranged between 37% (outer molecular layer) and 14% (*stratum oriens*; CA1). Finally, *synaptopodin* mRNA expression was studied using in situ hybridization, laser microdissection, and quantitative reverse transcriptase-polymerase chain reaction. Expression levels were comparable between all regions. These data demonstrate a lamina-specific distribution of Synaptopodin within dendritic segments of identified neurons. Within dendrites, the majority of Synaptopodin-positive puncta were located in spines where they represent spine apparatuses. We conclude, that this organelle is distributed in a region- and layer-specific manner in the mouse hippocampus and suggest that differences in the activity of afferent fiber systems could determine its distribution. J. Comp. Neurol. 487:227–239, 2005. © 2005 Wiley-Liss, Inc.

Indexing terms: synapse; plasticity; calcium store; EGFP; laser microdissection

Grant sponsor: Deutsche Forschungsgemeinschaft; Grant number: SFB 269; Grant number: SFB 505; Grant sponsor: Volkswagenstiftung; Grant number: I177282.

Carola A. Haas' present address is Experimental Epilepsy Research, University of Freiburg, D-79106 Freiburg, Germany.

Peter Mundel's present address is Department of Medicine, Mount Sinai School of Medicine, New York, NY 10029.

*Correspondence to: Thomas Deller, Institute of Clinical Neuroanatomy, J. W. Goethe University, Theodor-Stern-Kai 7, D-60590 Frankfurt/Main, Germany. E-mail: t.deller@em.uni-frankfurt.de

Received 3 August 2004; Revised 9 November 2004; Accepted 19 January 2005

DOI 10.1002/cne.20539

Published online in Wiley InterScience (www.interscience.wiley.com).

Synaptopodin is the first member of a class of proline-rich actin-associated proteins, which are not only found in the brain but also in kidney podocytes and different types of muscle cells (Mundel et al., 1997; Weins et al., 2001). So far, Synaptopodin is the only molecule of this class that has been detected in brain, where it is expressed in a 100-kDa isoform by adult spine-bearing telencephalic neurons (Mundel et al., 1997). Morphological analysis revealed that Synaptopodin is sorted to the spine compartment, where it is tightly associated with the spine apparatus (Mundel et al., 1997; Deller et al., 2000a,b, 2002), a Ca^{2+} -storing organelle (Gray, 1959; Fifikova et al., 1983; Spacek, 1985). Using mice homozygous for a targeted deletion of the *synaptopodin* gene, we could demonstrate recently that Synaptopodin is, in fact, an essential component of the spine apparatus (Deller et al., 2003): Synaptopodin-deficient mice lack spine apparatuses and show deficits in long-term potentiation and spatial learning. Thus, Synaptopodin and the spine apparatus organelle appear to be involved in synaptic plasticity of the adult brain.

In our previous studies on the distribution of Synaptopodin, we noted an uneven distribution pattern of Synaptopodin-positive puncta in the rodent hippocampus (Deller et al., 2000a,b, 2002). This pattern corresponds to the laminar organization of the hippocampus, which is generated by the layer-specific termination of extrinsic and intrinsic afferent fiber systems (Amaral and Witter, 1995). Of interest, the normal Synaptopodin distribution pattern is lost if the hippocampal cytoarchitecture is disrupted, for example, in reeler mice (Deller et al., 2002). On the basis of these data, we hypothesized that the immunolabeling pattern of Synaptopodin is generated by a layer-specific sorting of Synaptopodin along dendrites of hippocampal neurons (Deller et al., 2000a,b). This hypothesis, although highly plausible, is not easy to test, because it requires an extensive quantitative analysis of Synaptopodin-positive structures in dendrites of identified hippocampal principle cells. For such an analysis, classic methods used to identify and study single cells, such as electron microscopic reconstructions or the Golgi technique, are of limited use, because these methods cannot be used on a larger scale. In recent years, however, transgenic mice have been generated that express fluorescent proteins in single neurons of the brain (Feng et al., 2000). One of these mouse strains, the so-called Thy1GFP-M line, is of considerable interest, because it expresses enhanced green fluorescent protein (EGFP) in single principal neurons of the hippocampal formation. These neurons are intensely fluorescent and their dendrites are stained in a Golgi-like manner. Using Synaptopodin-immunostained hippocampal sections of these mice for three-dimensional confocal reconstruction, we could test on the cellular level whether Synaptopodin is differentially sorted along hippocampal dendrites.

With this goal in mind, we first verified our previous qualitative observations that Synaptopodin is differentially distributed in the hippocampus and performed a quantitative analysis of Synaptopodin puncta densities using confocal imaging techniques. We then excluded a partial presynaptic localization of Synaptopodin, using Synaptophysin and Synaptopodin immunofluorescent double-labeling. In a third step, we studied and quantified the distribution of Synaptopodin in single principal cells using three-dimensional confocal reconstructions of

Synaptopodin-immunostained and EGFP-labeled principal neurons. Finally, we excluded the possibility that differences in *synaptopodin* mRNA expression contributed to the regional differences in Synaptopodin-protein by measuring regional *synaptopodin* mRNA expression levels using in situ hybridization, laser capture microdissection (LMD), and quantitative reverse transcriptase-polymerase chain reaction (RT-PCR; Burbach et al., 2003).

MATERIALS AND METHODS

Animals and tissue preparation

For immunostaining, adult male C57BL/6 mice (3–6 months; $n = 7$) and adult male Thy1GFP transgenic mice (Thy1GFP-M line, Feng et al., 2000; 4 months; $n = 3$) housed under standard laboratory conditions were used. Mice were deeply anesthetized with an overdose of pentobarbital (300 mg/kg body weight) and transcardially perfused with 0.9% NaCl followed by 4% paraformaldehyde in phosphate buffered saline (PBS, pH 7.4). Brains were removed and post-fixed for 24 hours in 4% paraformaldehyde. Serial frontal sections (50 μm) were cut with a Vibratome (VT 1000S, Leica, Bensheim, Germany). All experiments were performed in agreement with the German law on the use of laboratory animals.

For in situ hybridization, adult male C57BL/6 mice (3–6 months; $n = 3$) were deeply anesthetized with an overdose of pentobarbital (300 mg/kg body weight) and transcardially perfused with 4% paraformaldehyde in 0.1 M phosphate buffer (PB), pH 7.4, for 20 minutes. Brains were removed and post-fixed in the same fixative for a few hours at 4°C followed by cryoprotection in 20% sucrose in 0.1 M PB, pH 7.4, at 4°C overnight. Cryostat sections (40 μm , coronal plane) of the hippocampus were processed for in situ hybridization as described previously (Deller et al., 2002).

For laser microdissection and quantitative RT-PCR, adult male C57BL/6 mice (3–6 months, $n = 3$) were killed using an overdose injection of pentobarbital (300 mg/kg body weight). Brains were removed, embedded in tissue freezing medium (Leica, Bensheim, Germany), and immediately flash-frozen in 2-methyl-butane at -40°C for short-term storage at -70°C or instant sectioning. Serial cryostat sections (thickness: 12 μm) of the septal portion of the hippocampus were cut and mounted on polytarthallene (PET) foil stretched on a metal frame (Leica). Sections were then fixed in ice-cold acetone for 3 minutes, dried on a heater at 40°C for 10 minutes, and subjected to histochemical staining.

Immunostaining

Free-floating hippocampal sections of C57BL/6 and Thy1GFP transgenic mice were incubated in 5% normal goat serum, 0.5% Triton X-100 in PBS for 1 hour to reduce unspecific staining and subsequently incubated for 2 days at 4°C in an affinity purified anti-Synaptopodin antiserum (Mundel et al., 1997); 1:1,500, 1% bovine serum albumin, 0.1% Triton X-100 in PBS. After three washing steps in PBS, sections were incubated with an Alexa 568-labeled goat anti-rabbit secondary antibody (Molecular Probes, Eugene, OR; 1:1,000, 1% bovine serum albumin, 0.1% Triton X-100) at room temperature for 2 hours. Sections were washed again, transferred onto glass slides, and mounted under glass coverslips with anti-fading mount-

ing medium (DAKO Fluorescent Mounting Medium; Dako, Hamburg, Germany). For double immunolabeling, sections were incubated in a mixture of rabbit anti-Synaptopodin antiserum and mouse anti-Synaptophysin antibody (MAB 5258; Chemicon, Temecula, CA). After washing, sections were incubated first with anti-rabbit secondary antibody, washed again, and then incubated with anti-mouse secondary antibody.

Confocal imaging and quantitative analysis of Synaptopodin puncta densities

Synaptopodin puncta densities were analyzed in three sections per animal (500 μm , 1,000 μm , and 1,500 μm from the septal pole of the hippocampal formation) using a Zeiss LSM 510 laser scanning microscope, a Zeiss 63 \times oil immersion lens (NA 1.4), and 2 \times scan zoom. Detector gain and amplifier offset were initially set to obtain pixel densities within a linear range. Per section, 19 frames (frame size, 30 $\mu\text{m} \times 30 \mu\text{m} \times 1 \mu\text{m}$) were sampled in the dentate gyrus (hilus, granule cell layer, inner-, middle-, and outer molecular layer of the infra- as well as the suprapyramidal blade of the dentate gyrus), area CA3 (*strata oriens, pyramidale, lucidum, radiatum, and lacunosum-moleculare*), and area CA1 (*strata oriens, pyramidale, radiatum, and lacunosum-moleculare*; Fig. 1A–D). Images were recorded at tissue levels (3–5 μm below the surface of the section) where immunostaining for Synaptopodin was optimal, as confirmed in z-stacks throughout the entire section. All images were recorded using exactly the same settings. Quantitative analysis of confocal images was performed using the ImageJ software package (Fig. 1E–G; program available from <http://rsb.info.nih.gov/ij>). After standardization of the image analysis method (see Results section), the following parameters were chosen for analysis: threshold level 50; minimum size 5 pixels. All objects defined by these parameters were counted automatically by the software. Values for threshold as well as minimum object size were kept constant for all measurements. The number of positive puncta and the standard error of the mean (SEM) were calculated and expressed as mean number of puncta per 1,000 $\mu\text{m}^3 \pm 2 \times \text{SEM}$. Layer-specific densities of Synaptopodin-positive puncta were compared within each hippocampal subfield. Layers were tested against each other for statistical significance using analysis of variance (ANOVA) followed by Bonferroni's multiple comparisons post hoc test (significance level $P \leq 0.05$).

Confocal imaging and quantitative analysis of Synaptopodin puncta in EGFP-labeled hippocampal principle cells

Hippocampal sections from the dorsal hippocampus of Thy1GFP transgenic mice ($n = 3$) stained for Synaptopodin were used to study the distribution of Synaptopodin-positive puncta in identified principal cells. In these sections, EGFP-labeled granule cells, CA3 pyramidal cells, and CA1 pyramidal cells were randomly selected. To ensure optimal immunolabeling, only those dendritic segments were used for analysis, which were located in the zone of optimal Synaptopodin immunostaining (antibody penetration into the tissue was verified in each section using z-stack analysis). In all cases, secondary or tertiary dendritic segments were used. Confocal image stacks were recorded in the dentate gyrus (inner- and outer-molecular layer), area CA3 (*strata oriens, radiatum, and lacunosum-*

moleculare), and area CA1 (*strata oriens, radiatum, and lacunosum-moleculare*), using a Zeiss 63 \times oil immersion lens (NA 1.4) and 4 \times scan zoom. Up to 70 images with a z-interval of 0.15 μm were recorded per stack. After data acquisition, dendritic segments were three dimensionally analyzed by a second investigator who was blind to the location of the dendritic segments. To optimally demonstrate the subcellular localization of Synaptopodin-immunoreactive structures, selected images were further processed by three-dimensional deconvolution (AutoDeblur software, AutoQuant, Troy, New York) and three-dimensional surface rendering (Imaris software, Bitplane, Switzerland).

First, these data were used to determine the percentage of Synaptopodin-positive puncta associated with dendritic spines or dendritic shafts. Synaptopodin-positive puncta were considered to be located in spines, if the three-dimensional analysis revealed part of the Synaptopodin-positive structure within the spine head or neck. They were considered to be located within dendritic shafts, if three-dimensional analysis revealed no spine-association.

Next, the percentage of Synaptopodin-positive spines was determined. For this, the total number of spines and the total number of Synaptopodin-positive spines were counted in each dendritic segment. The percentage of Synaptopodin-containing spines and the SEM were calculated and expressed as mean percentage of positive spines $\pm 2 \times \text{SEM}$. Layers within each hippocampal subfield were tested against each other for statistical significance using ANOVA followed by Bonferroni's multiple comparisons post hoc test (significance level $P \leq 0.05$).

In situ hybridization

For in vitro transcription, a human synaptopodin cDNA (Mundel et al., 1997) was subcloned into the pBluescript SK (-) vector (Stratagene, La Jolla, CA). Digoxigenin (DIG)-labeled antisense and sense cRNA probes were prepared from the linearized plasmid using T3 and T7 RNA polymerases, respectively. In vitro transcription was performed with 1 μg of plasmid template in the presence of ATP, GTP, CTP, and digoxigenin-11-UTP (DIG-11-UTP, Roche Diagnostics, Mannheim, Germany), RNasin, transcription buffer (pH 8.0) and T3 or T7 RNA polymerase for 2 hours at 37°C according to the manufacturer's recommendations (Roche Diagnostics, Mannheim, Germany). The DIG-labeled synaptopodin cRNA probes (ca. 2,000 bases) were treated by alkaline hydrolysis to reduce the size to approximately 250 bases following standard protocols.

For in situ hybridization histochemistry, cryostat sections were rinsed once in 2 \times standard saline citrate (SSC) and were pretreated in a 1:1 mixture of 2 \times SSC:hybridization buffer (50% formamide, 4 \times SSC, 50 mM NaH_2PO_4 , 250 $\mu\text{g}/\text{ml}$ heat-denatured salmon sperm DNA, 100 $\mu\text{g}/\text{ml}$ tRNA, 5% dextran sulfate, and 1% Denhardt's solution) for 15 minutes and prehybridized in hybridization buffer for 60 minutes at 45°C. Hybridization was performed in the same buffer including 100 ng/ml of DIG-labeled antisense or sense *synaptopodin* cRNA probes, respectively, at 55°C overnight. After hybridization, the brain sections were washed in 2 \times SSC (2 \times 15 minutes) at room temperature; 2 \times SSC and 50% formamide, 0.1 \times SSC and 50% formamide for 15 minutes at 65°C each; and finally in 0.1 \times SSC (2 \times 15 minutes) at 65°C. Immunological detection of DIG-labeled hybrids with anti-DIG-AP (anti-

digoxigenin antibody from sheep conjugated with alkaline phosphatase) was performed as recommended by the manufacturer (Roche Diagnostics, Mannheim, Germany). Colorimetric detection was accomplished using nitroblue tetrazolium (NBT) and 5-bromo-4-chloro-3-indolylphosphate (BCIP). Development of the color reaction was performed in the dark and stopped by transfer into 10 mM Tris-HCl, pH 8.0, and 1 mM ethylenediaminetetraacetic acid. Tissue sections were mounted onto glass slides and embedded in Moviol (Merck, Darmstadt, Germany).

Laser microdissection

For detection of cell layers in the hippocampus, histochemical staining was performed as described previously (Burbach et al., 2003). Briefly, sections were incubated with 1% toluidine blue (Merck, Darmstadt, Germany) in RNase-free water for 3 minutes at room temperature. After differentiation in 75% ethanol in DEPC water, the sections were dried and immediately subjected to LMD.

For LMD, PET foil metal frames were mounted on a Leica AS LMD system with the section facing downward. After adjusting intensity, aperture, and cutting velocity, the pulsed ultraviolet laser beam was carefully directed along the borders of the respective hippocampal cell layer. For each serial section, granule cell layer as well as CA1 and CA3 regions were collected separately. The area cut was then transferred by gravity alone into a microcentrifuge tube cap placed directly underneath the section. The tube cap was filled with a guanidine isothiocyanate (GITC)-containing buffer (Buffer RLT, RNeasy Mini Kit, Qiagen, Hilden, Germany) to ensure isolation of intact RNA. Tissue collection was verified by inspecting the tube cap. RNA isolation, DNA digestion, and reverse transcription were performed as described previously (Burbach et al., 2003). Integrity of the isolated RNA was determined using the Agilent RNA 6000 Pico Lab Chip (Agilent Technologies, Waldbronn, Germany). Only RNA with clearly distinguishable ribosomal peaks and without a shift in RNA size distribution to small size fragments was used.

Quantitative RT-PCR

cDNAs were subjected to PCR using the Abi Prism 7000 Sequence Detection System (Applied Biosystems; Darmstadt, Germany) and TaqMan Universal PCR Master Mix (Applied Biosystems). The following mouse-specific *synaptopodin* primers were selected using Primer Express software (Applied Biosystems): *synaptopodin* sense primer, 5'-GCCAGGGACCAGCCAGATA-3'; *synaptopodin* antisense primer, 5'-AGGAGCCCAGGCCCTTCTCT-3'; *synaptopodin* probe, 5'-AAGCCCCATGATGGGAAGACGACAGTT-3'. For normalization of Ct values to an endogenous control the following eukaryotic 18S ribosomal RNA primers were used: 18S rRNA sense primer, 5'-CGGCTACCACATC-CAAGGAA-3'; 18S rRNA antisense primer, 5'-GCTGGAATTACCGCGGCT-3'; 18S rRNA probe, 5'-TGCTGGCACCAGACTTGCCCTC-3'. Amplicon sizes for *synaptopodin* and 18S rRNA were 73 bp and 181 bp, respectively. Probes were labeled with 6-carboxyfluorescein (FAM) at the 3'-end and with 6-carboxy-tetramethyl-rhodamine (TAMRA) at the 5'-end. For both the amplification of mouse *synaptopodin* and 18S cDNA, a standard amplification program was used (1 cycle of 50°C for 2 minutes, 1 cycle of 95°C for 10 minutes, 45 cycles of 95°C for 15 seconds, and 60°C for 1 minute). Using standard curves of serial control cDNA dilutions a relative quantitation of target cDNA expressed in

relative x-fold differences was performed. All quantitations were normalized to an endogenous control (18S rRNA) to account for variability in the initial concentration and in the conversion efficiency of the reverse transcription reaction. Statistical analysis was performed using SPSS for Windows (SPSS, Munich, Germany), and Student *t* test was used to test for statistical significances ($P \leq 0.05$).

Digital illustrations

Confocal images were exported from the Zeiss LSM image browser and stored as TIFF files. Conventional fluorescence images were acquired using an attached Spot2 digital camera (Diagnostic Instruments, Sterling Heights, MI) and stored as TIFF files. Figures were prepared using Photoshop 6.0 graphics software (Adobe, San Jose, CA). Image brightness, contrast, and sharpness were adjusted. For overview figures (Figs. 4B, 5A,C), confocal image stacks were projected onto the X–Y plane using the projection function of the Zeiss LSM image browser.

RESULTS

Synaptopodin immunostaining in the mouse hippocampus

Synaptopodin immunostaining of mouse hippocampus revealed regional and laminar differences in the distribution of Synaptopodin protein (Fig. 1A–D), as previously described (Deller et al., 2002). Using high-magnification confocal laser scanning microscopy, Synaptopodin immunostaining was resolved into single immunofluorescent puncta, which could readily be distinguished. Similarly, laminar differences in Synaptopodin immunostaining were revealed as differences in Synaptopodin puncta densities (Figs. 1E, 2A–D). Because Synaptopodin-immunoreactive puncta were clearly distinct, a computer-based image analysis program (ImageJ) was used to verify and quantify the layer-specific differences in Synaptopodin puncta densities (Fig. 1F,G).

Quantification of Synaptopodin-immunoreactive puncta densities: methodological aspects

Although computerized image analysis programs are highly convenient and widely used tools for quantitative analysis in many fields of science, they need to be carefully validated and standardized before analysis. Especially, the parameters chosen for analysis may influence the numerical value of the data set. Thus, we validated the image analysis method for Synaptopodin immunolabeling and performed a series of methodological experiments in which threshold level (background suppression) and pixel size (automatic particle detection) were systematically altered (data not shown). These experiments revealed that the absolute values obtained for Synaptopodin-puncta densities noticeably depended on the parameters chosen by the investigator, i.e., the biological interpretation of the image. In contrast, relative differences between layers were robust within a very broad range of parameters (threshold level, 10–200; pixel size, 1–10) and remained statistically significant at comparable error levels. We conclude from these observations that absolute density values obtained with this method should be regarded with some caution. The relative differences between the layers,

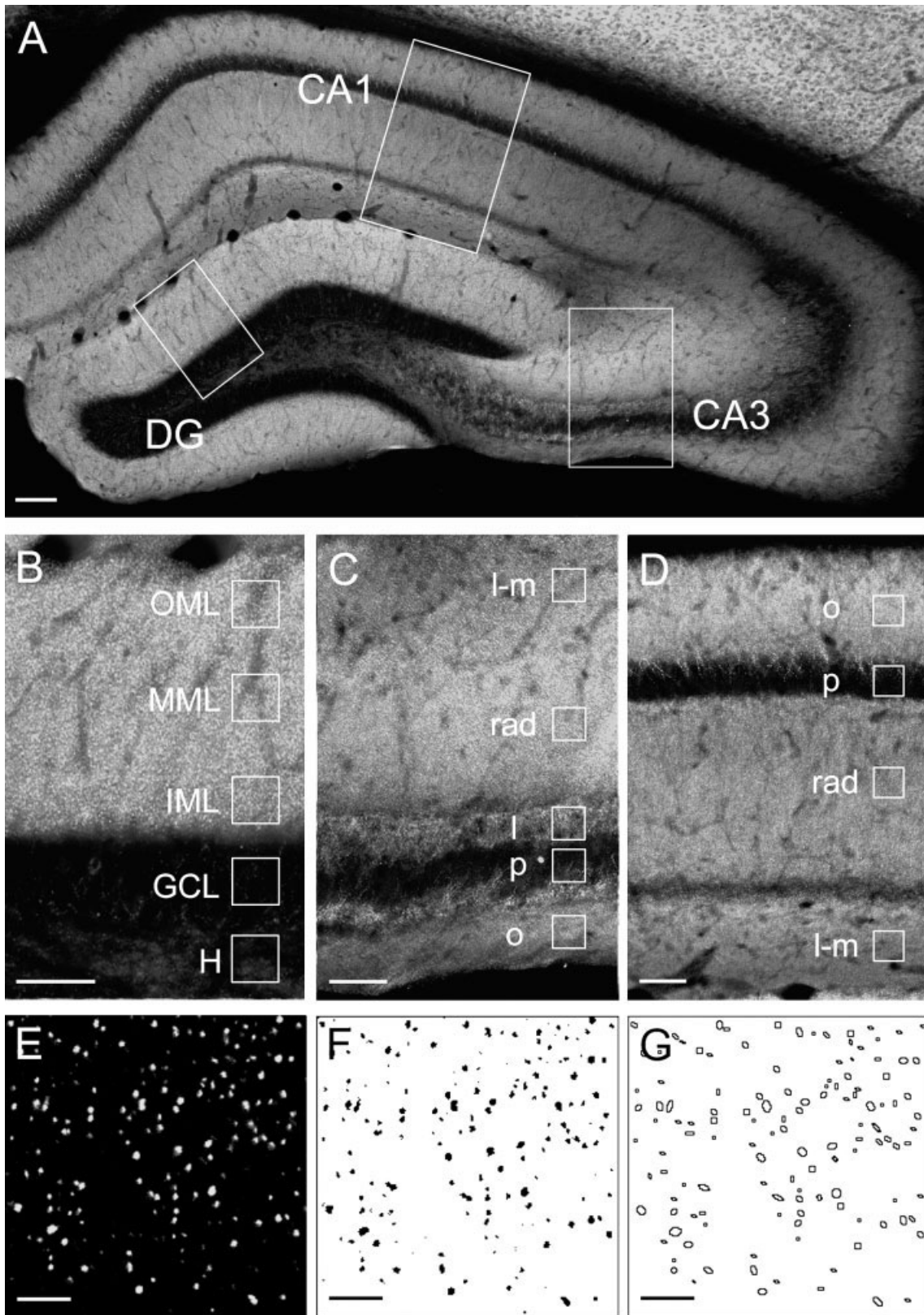


Fig. 1. Quantification of Synaptopodin puncta densities in the mouse hippocampus. **A:** Frontal section of mouse hippocampus stained for Synaptopodin. Note layer- and region-specific differences in Synaptopodin immunoreactivity. **B–D:** Higher magnification of the dentate gyrus (B), area CA3 (C), and area CA1 (D); the densities of Synaptopodin-positive puncta in different hippocampal layers were determined in representative areas ($30\ \mu\text{m} \times 30\ \mu\text{m} \times 1\ \mu\text{m}$), indicated by frames in B,C,D. **E:** Higher magnification confocal image, showing single immunoreactive puncta, taken from the IML. **F:** Bi-

nary image of E, generated with the image analysis software by defining a lower threshold. Objects with lower intensity values than the threshold were set equal to background. **G:** Image showing the outlines of all particles, which were counted by the software. DG, dentate gyrus; GCL, granule cell layer; H, hilus; IML, inner molecular layer; l, *stratum lucidum*; l-m, *stratum lacunosum-moleculare*; MML, middle molecular layer; o, *stratum oriens*; OML, outer molecular layer; p, *stratum pyramidale*; rad, *stratum radiatum*. Scale bars = $100\ \mu\text{m}$ in A; $50\ \mu\text{m}$ in B–D; $5\ \mu\text{m}$ in E–G.

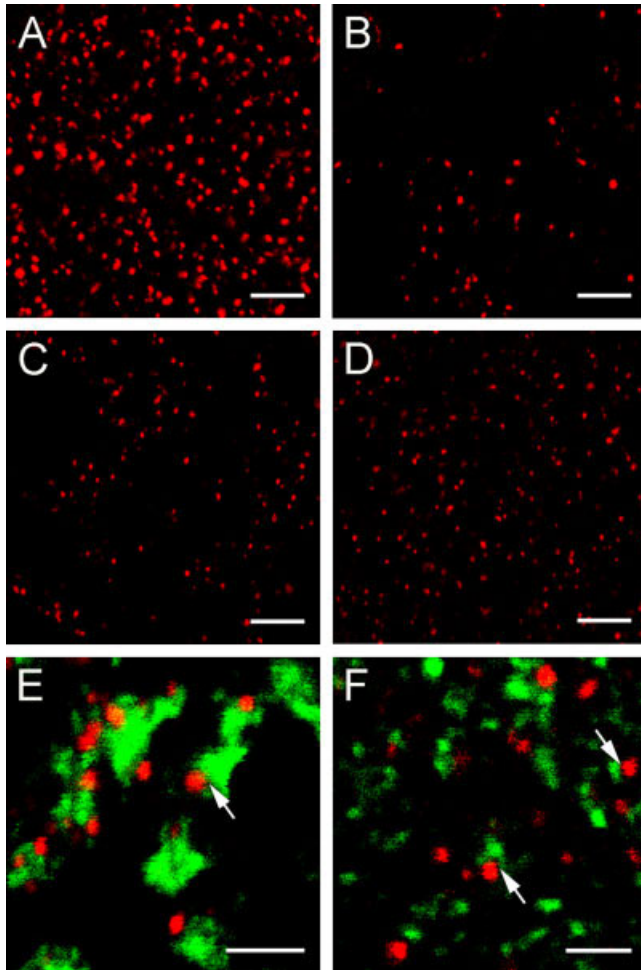


Fig. 2. Laminar differences in Synaptopodin-positive puncta densities in the mouse hippocampus. **A–D**: High-magnification confocal images, showing single Synaptopodin-positive puncta, taken from middle molecular layer (A), hilus (B), *stratum lucidum* of area CA3 (C), and *stratum radiatum* of area CA1 (D). Differences between layers are clearly visible. **E,F**: Double-immunolabeling for Synaptopodin (red) and Synaptophysin (green) in *stratum lucidum* of area CA3 (E) and *stratum radiatum* of area CA1 (F). Note close apposition of Synaptopodin- and Synaptophysin-positive structures (arrows). Synaptophysin-positive structures in E are large mossy fiber boutons in contact with complex spines of CA3 pyramidal cells. Scale bars = 5 μm in A–D; 2 μm in E,F.

however, are fairly independent of these variables and, thus, reliable.

Quantitative analysis of Synaptopodin-immunoreactive puncta densities

Synaptopodin densities were obtained for each layer and tested for significance against all other layers within a given subfield. In the following, the data are given as mean number of puncta per $1,000 \mu\text{m}^3 \pm 2 \times \text{SEM}$ for each layer. All data were obtained in the dorsal hippocampus (see Materials and Methods section).

In the dentate gyrus (Fig. 3), the number of Synaptopodin-immunoreactive puncta was highest in the molecular layer, i.e., the zone of the granule cell dendrites.

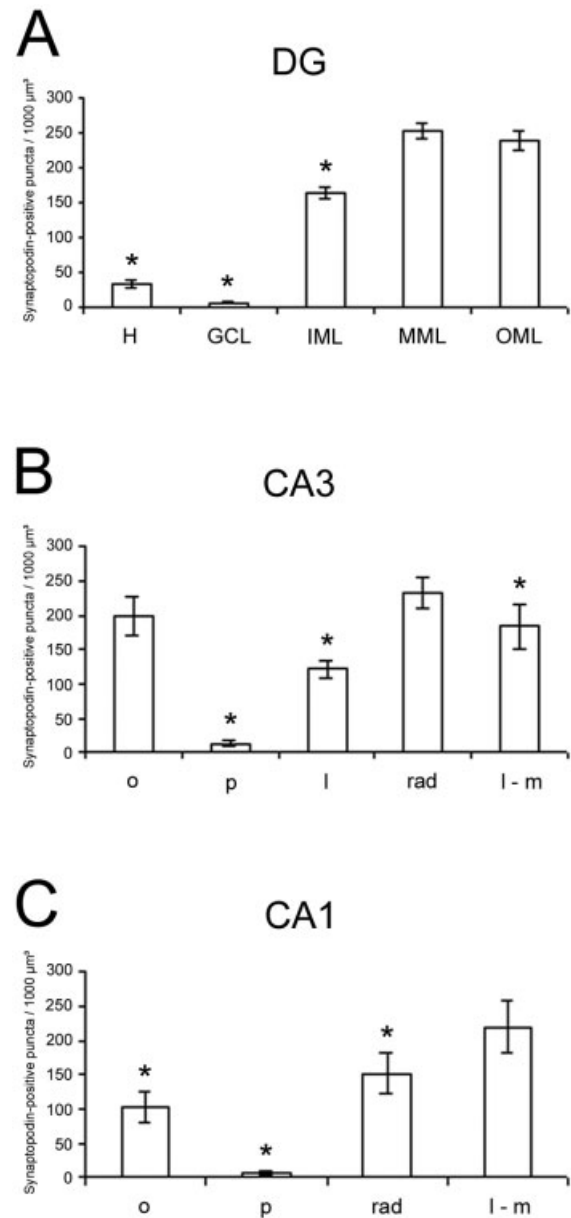


Fig. 3. Layer- and region-specific distribution of Synaptopodin. **A–C**: Mean densities of Synaptopodin-positive puncta per $1,000 \mu\text{m}^3 (\pm 2 \text{ SEM})$ shown for different layers of dentate gyrus (DG; A), area CA3 (B), and area CA1 (C). The layer with the highest puncta density was tested against the other layers of the same subfield. Asterisks indicate significant differences in puncta densities between the subfield layers. GCL, granule cell layer; H, hilus; IML, inner molecular layer; l, *stratum lucidum*; l-m, *stratum lacunosum-moleculare*; MML, middle molecular layer; o, *stratum oriens*; OML, outer molecular layer; p, pyramidal cell layer; rad, *stratum radiatum*.

Of interest, differences between the zones of the molecular layer could be detected: The number of Synaptopodin-positive puncta was significantly higher in the middle and outer molecular layer (252.7 ± 11.8 and 238.4 ± 14 puncta per $1,000 \mu\text{m}^3 \pm 2 \times \text{SEM}$, respectively) compared with the inner one third (163.5 ± 9.5). Only few immunoreac-

tive puncta were counted in the hilus (32.2 ± 5.1) and even less were found in the granule cell layer (5.8 ± 1.4). No significant differences were found between the supra- and infrapyramidal blade of the dentate gyrus.

In hippocampal subfield CA3 (Fig. 3), the numbers of Synaptopodin-positive puncta in the dendritic fields were within the range of those found in the molecular layer of the dentate gyrus: *stratum oriens* (198.7 ± 28.9) and *stratum radiatum* (232.3 ± 22.1). Although numbers were not significantly different between these layers, the highest number of puncta was observed in the *stratum radiatum*. *Stratum lucidum* (122 ± 12.5) and *stratum lacunosum-moleculare* (183.5 ± 32.5) showed significantly less Synaptopodin-positive puncta than *stratum radiatum*. The number of Synaptopodin-positive puncta in *stratum pyramidale* (12.8 ± 4.1) was slightly, but significantly higher than the number of puncta found in the granule cell layer of the dentate gyrus.

In area CA1 (Fig. 3), only the number of Synaptopodin-positive puncta in *stratum lacunosum-moleculare* (220 ± 38.9) was within the range of those found in the molecular layer of the dentate gyrus or in *stratum radiatum* and *stratum oriens* of CA3. In *stratum oriens* (102 ± 22.4) and *stratum radiatum* (152.3 ± 30), the number of Synaptopodin-positive puncta was significantly lower compared with the same layers of area CA3. The number of Synaptopodin-positive puncta in *stratum pyramidale* (6.5 ± 2.1) was similar to the number found in the granule cell layer of the dentate gyrus.

Synaptopodin and Synaptophysin double-immunofluorescence staining

Double-immunofluorescence for Synaptopodin and the presynaptic marker molecule Synaptophysin was performed to exclude a partial presynaptic localization of Synaptopodin in the hippocampus. This appeared to be necessary in the context of this study, because a partial presynaptic localization of Synaptopodin could explain the laminar pattern of Synaptopodin-immunostaining in the mouse hippocampus. In our material, however, Synaptophysin and Synaptopodin never colocalized. Rather, Synaptophysin-positive terminals and Synaptopodin-positive puncta were frequently opposed, suggesting that these two structures are part of the same axospinous synapse (Fig. 2E,F). This relationship was especially impressive in *stratum lucidum* of area CA3, where specialized axon terminals are formed by the granule cell axons, the mossy fibers. These terminals form very large boutons, which engulf specialized spines of CA3 pyramidal cells, the so called thorny excrescences (Amaral and Witter, 1995). These spines almost invariably contain a spine apparatus in one or more of their finger-like processes (Hamlyn, 1962; Deller et al., 2000a; Capani et al., 2001). Double-immunofluorescence for Synaptopodin and Synaptophysin nicely revealed the relationship between the mossy fiber boutons and the spine-apparatus containing Synaptopodin-positive thorny excrescences (Fig. 2E). In none of these cases, however, did we observe a colocalization of the two markers.

Cellular distribution of Synaptopodin-positive structures in hippocampal principal cells

Using Synaptopodin-immunostained sections of Thy1GFP transgenic mouse hippocampus, the cellular distribution of Synaptopodin could be determined. This

analysis was limited to hippocampal principal cell types that were EGFP labeled in the transgenic mouse strain: dentate granule cells, CA3 pyramidal cells, and CA1 pyramidal cells. The morphology of these neurons is indistinguishable from the morphology of hippocampal neurons found in controls (M. Vuksic, D. Del Turco, T. Deller, unpublished observations). Dendritic segments of identified cells were analyzed in the various hippocampal laminae using three-dimensional reconstruction methods (Figs. 4A–D, 5).

We first wanted to clarify the location of Synaptopodin-positive structures within single neurons. Although our previous electron microscopic studies had primarily revealed Synaptopodin in spines where it was associated with the spine apparatus, Synaptopodin immunoreactivity was also observed in the dendritic shafts of some neurons (Deller et al., 2000a, 2002). Using three-dimensional confocal analysis (Figs. 4C, 5) and computer-aided dendritic reconstruction (Fig. 4D) of Synaptopodin-positive structures within EGFP-labeled principal cell dendrites, we found that more than 95% of Synaptopodin-positive puncta within a dendritic segment were located in spines rather than the dendritic shaft (Table 1). This finding was the case for all laminae, with the notable exception of *stratum lacunosum-moleculare* of area CA1, where 18.5% of Synaptopodin-positive puncta were found in dendritic shafts (Table 1). Of interest, Synaptopodin-positive puncta were located at variable positions within spines (Fig. 4C): Some were found exclusively in the spine head, others extended from the spine head into the neck, whereas again others were found in the spine neck or extended from the spine neck into the dendritic shaft.

Laminar distribution of Synaptopodin-positive spines along hippocampal principal cell dendrites

Next, we wanted to know the percentage of dendritic spines containing a Synaptopodin-positive structure. For this analysis, we used the same data set as outlined in the previous paragraph and exclusively analyzed the dendritic spine population. Significant layer-specific differences in the percentage of Synaptopodin-positive spines were revealed (Fig. 4E). The highest percentage of Synaptopodin-positive spines was found in the outer and middle molecular layer of the dentate gyrus, where 36.6% of all spines contained Synaptopodin. The lowest percentage of Synaptopodin-positive spines was found in *stratum oriens* of CA1, where only 13.9% of all spines contained a Synaptopodin-positive structure. Thus, the percentage of Synaptopodin-positive spines was 2.5 times higher in some dendritic segments compared with others. In CA1, a similar relationship was found even between different dendritic segments of the same cell type: The percentage of Synaptopodin-positive spines was almost 2.3 times higher in *stratum lacunosum-moleculare* (31.7%) compared with *stratum radiatum* (14.3%) and *stratum oriens* (13.9%).

Because this study focuses on the laminar distribution of Synaptopodin-positive spines in the mouse hippocampus, a detailed analysis of individual spines was not performed. The precise location of Synaptopodin-positive structures within individual spines and the length profiles of the Synaptopodin-positive spines are currently being

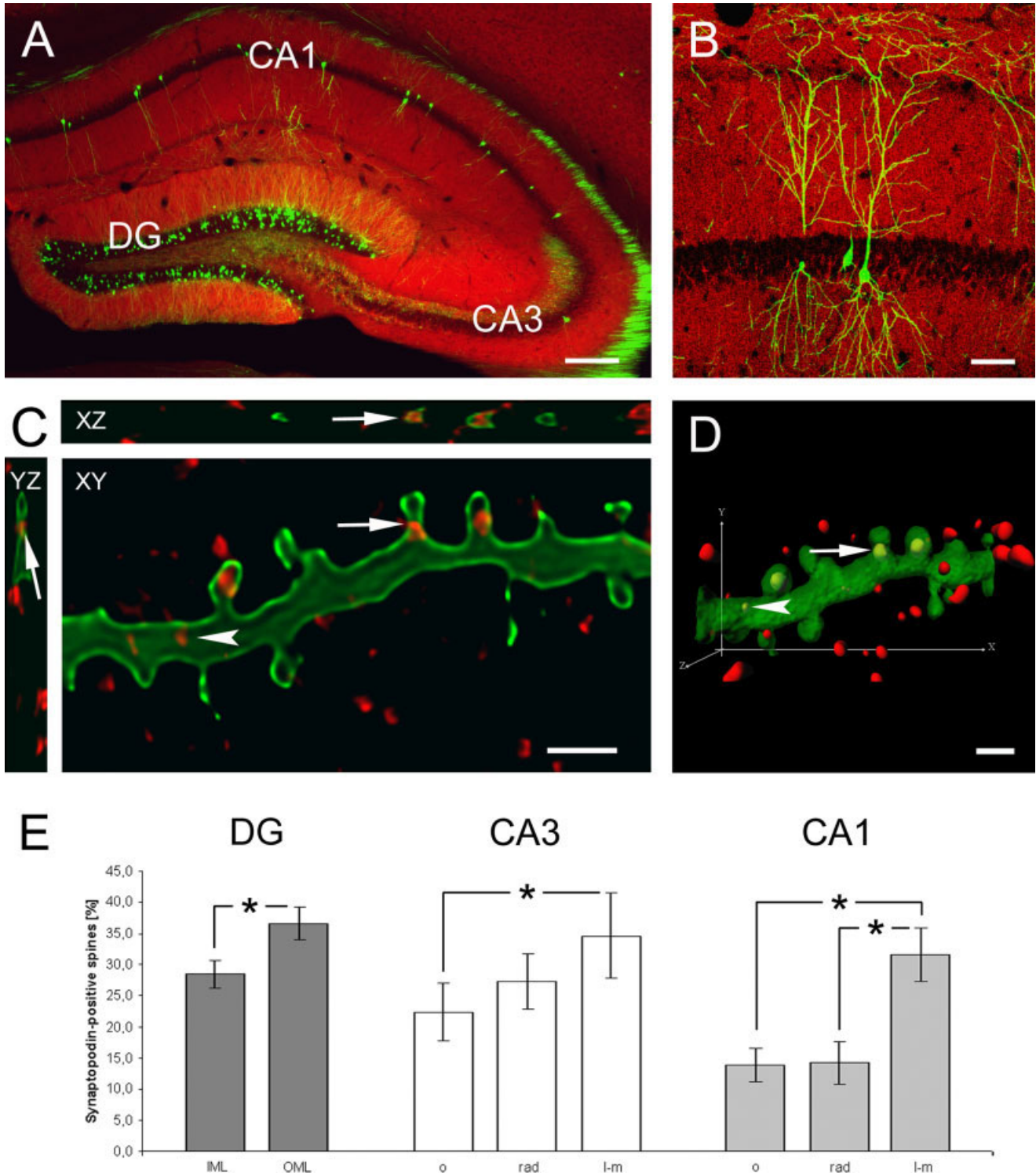


Fig. 4. Laminar distribution of Synaptopodin-positive puncta in dendritic segments of identified hippocampal principal cells. **A:** Frontal section of the hippocampus (Thy1GFP transgenic mouse) stained for Synaptopodin (red). Several enhanced green fluorescent protein (EGFP)-labeled neurons (green) are visible in the dentate gyrus (DG), in subfield CA3, and in subfield CA1. **B:** Higher magnification of EGFP-labeled neurons in area CA1. The entire dendritic arbor of EGFP-labeled neurons is stained in a Golgi-like manner. **C:** Three dimensional analysis of identified dendritic segments was performed using confocal imaging. The intracellular location of Synaptopodin puncta could be resolved by analyzing single sections from a confocal image stack in the X-Y, X-Z, and Y-Z planes. In this pyramidal cell dendrite (CA1, *stratum oriens*), several Synaptopodin-positive puncta

are located in spines. The arrows indicate a Synaptopodin-positive structure located within a spine neck. Occasionally, Synaptopodin-positive puncta were found in dendrites (arrowhead). **D:** Three-dimensional reconstruction of the dendritic segment shown in C. Synaptopodin-positive structures located within the EGFP-labeled neuron are coded in yellow. **E:** Percentage of Synaptopodin-positive spines (± 2 SEM) in identified dendritic segments (IML, inner molecular layer; OML, outer molecular layer; l-m, *stratum lacunosum-moleculare*; o, *stratum oriens*; rad, *stratum radiatum*). Asterisks indicate significant differences between the layers. DG, dentate gyrus; CA3, hippocampal subfield; CA1, hippocampal subfield. Scale bars = 200 μm in A; 50 μm in B; 1 μm in C,D.

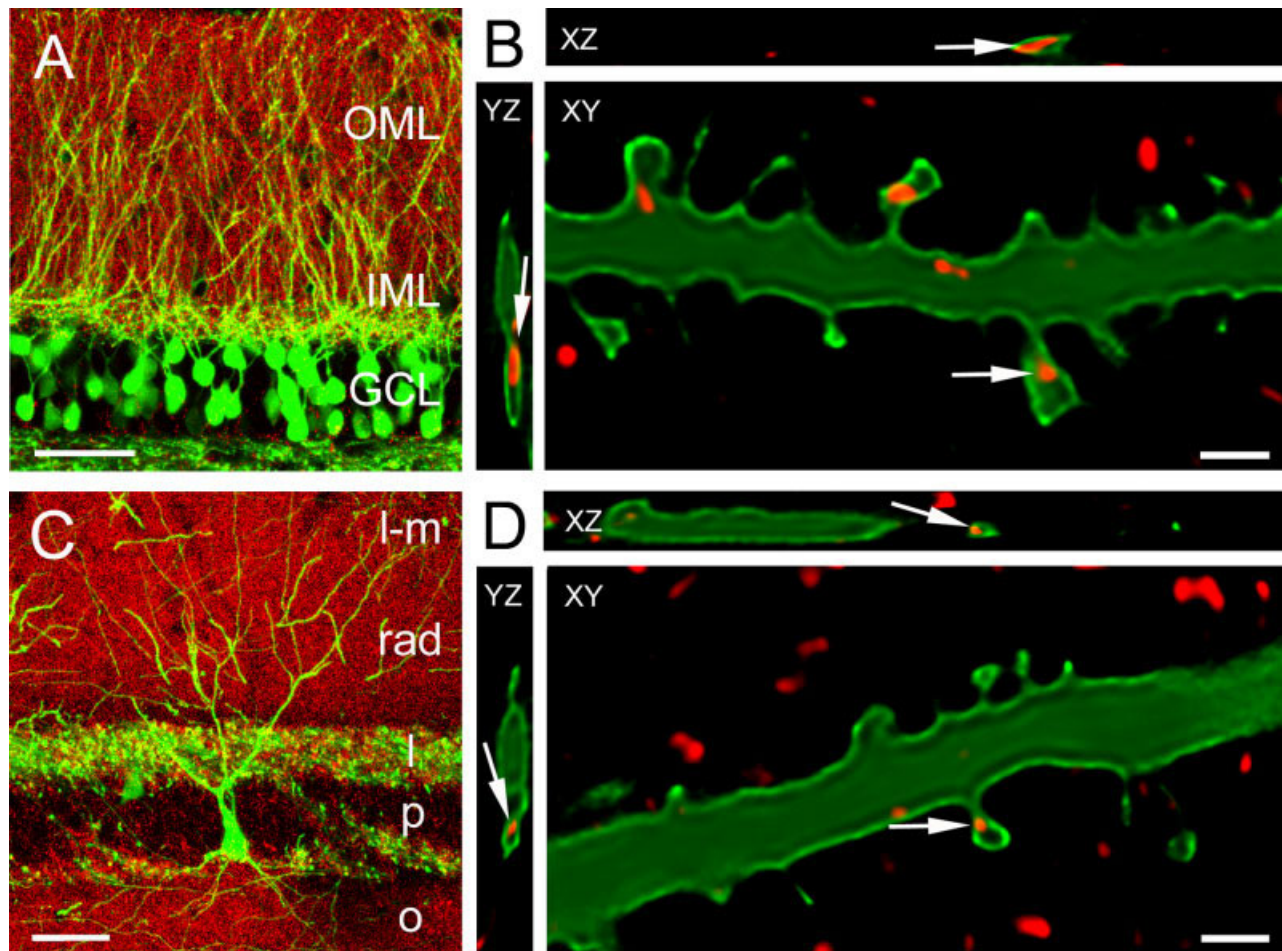


Fig. 5. Distribution of Synaptopodin-positive puncta in dendritic segments of enhanced green fluorescent protein (EGFP)-labeled granule cells and CA3 pyramidal cells. **A:** Portion of the dentate gyrus of a Thy1GFP transgenic mouse stained for Synaptopodin (red). Several granule cells in the granule cell layer (GCL) are EGFP-labeled (green). A dendritic segment located in the outer two thirds of the molecular layer (OML) is illustrated in **B**. **B:** Higher magnification of an EGFP-labeled granule cell dendrite in the OML. Single sections from a confocal image stack in X-Y, X-Z, and Y-Z plane, respectively. Arrows point to a Synaptopodin-positive dot located within a large spine. **C:** Portion of hippocampal subfield CA3 stained for Synaptopodin.

An EGFP-labeled pyramidal cell is illustrated. Note the EGFP-positive mossy fiber boutons in *stratum lucidum* (l). A dendritic segment located in *stratum radiatum* (rad) is illustrated at higher magnification in **D**. **D:** Higher magnification of an EGFP-labeled granule cell dendrite in *stratum radiatum*. Single sections from a confocal image stack in X-Y, X-Z, and Y-Z plane, respectively. The arrows indicate a Synaptopodin-positive structure located within a spine neck. IML, inner molecular layer; l-m, *stratum lacunosum-moleculare*; o, *stratum oriens*; p, *stratum pyramidale*. Scale bars = 50 μ m in A,C; 1 μ m in B,D.

TABLE 1. Percentage of Synaptopodin-Positive Puncta in Dendritic Shafts and Spines¹

Area	DG		CA3			CA1		
	IML	OML	o	rad	l-m	o	rad	l-m
n	333	477	161	198	170	108	114	118
Spine [%]	97.9 ± 0.4	97.9 ± 1.9	95.2 ± 0.9	96.9 ± 3.1	96.2 ± 2.6	97.7 ± 2.1	100 ± 0.0	81.5 ± 2.1
Shaft [%]	2.1 ± 0.4	2.1 ± 1.9	4.8 ± 0.9	3.1 ± 3.1	3.8 ± 2.6	2.3 ± 2.1	0 ± 0.0	18.5 ± 2.1

¹DG, dentate gyrus; IML, inner molecular layer; l-m, *stratum lacunosum-moleculare*; o, *stratum oriens*; OML, outer molecular layer; rad, *stratum radiatum*.

analyzed for the different hippocampal neuron types and will be communicated in a separate report.

Synaptopodin mRNA-expressing cells as revealed by in situ hybridization

In situ hybridization for *synaptopodin* mRNA was used to identify *synaptopodin*-expressing cells. The sense con-

trol showed no labeling (not shown). In the dentate gyrus and hippocampus, *synaptopodin* expression was found primarily within the principal cell layers, i.e., the granule cell layer, subfield CA3, and subfield CA1 (Fig. 6A). In addition, some *synaptopodin* mRNA-expressing cells could be detected in the hilus, in *stratum lucidum* of CA3, and, occasionally, in the white matter areas, where spine bear-

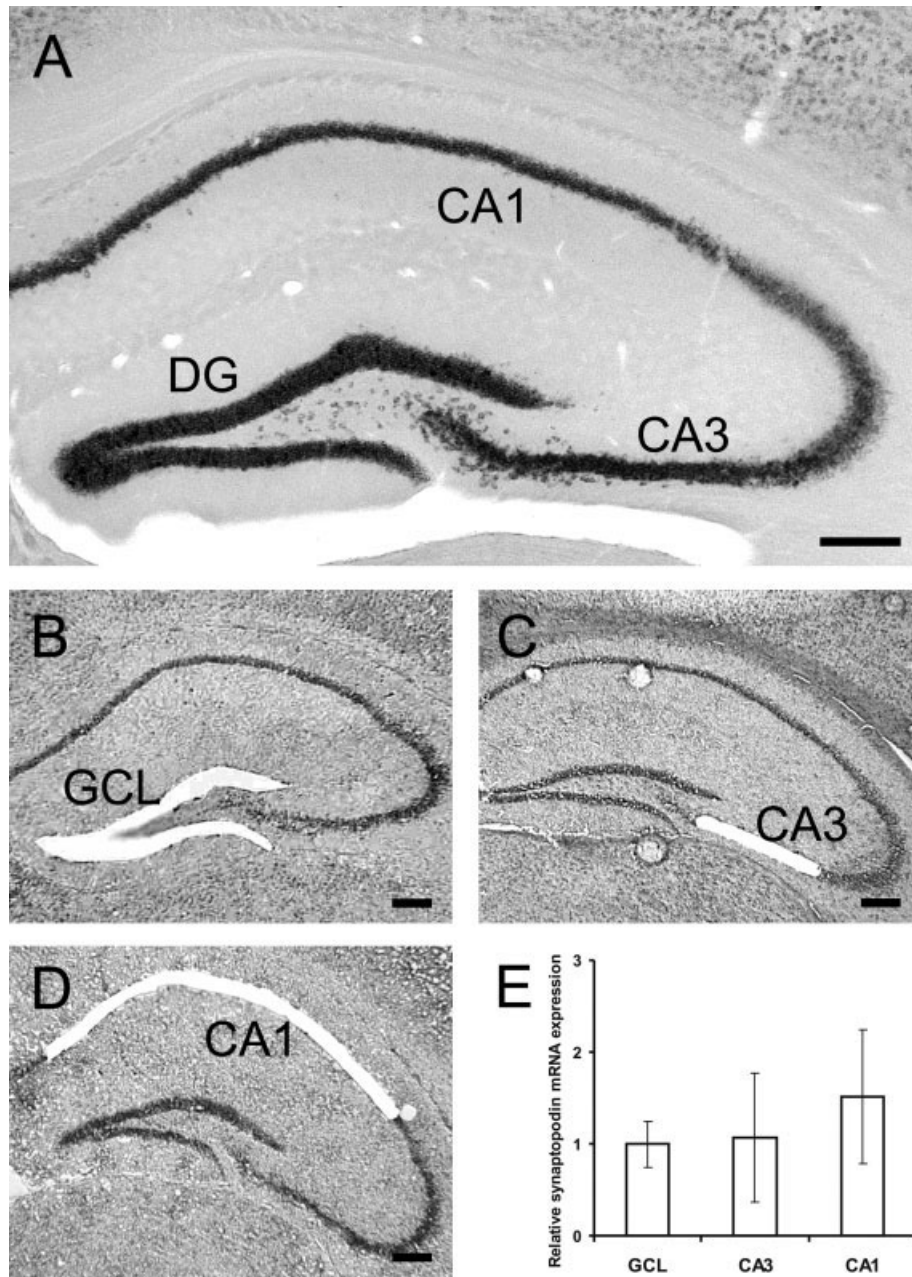


Fig. 6. Quantification of *synaptopodin* mRNA expression in hippocampal principal cells. **A:** Nonradioactive in situ hybridization for *synaptopodin* mRNA. Note the strong hybridization signal in the principal cell layers. **B–D:** Toluidine blue-stained sections used for laser microdissection. The principal cell layers of the hippocampus can readily be identified. Portions of the granule cell layer (GCL; B), the pyramidal cell layer of area CA3 (C), and the pyramidal cell layer of area CA1 (D) were microdissected for quantification of *synaptopodin*

synaptopodin mRNA. **E:** Relative *synaptopodin* mRNA expression, assessed by quantitative reverse transcriptase-polymerase chain reaction. Levels of *synaptopodin* mRNA expression (\pm SD) in pyramidal cell layers of area CA1 and CA3 are shown relative to expression levels in the granule cell layer. No significant differences in expression levels could be detected between the three hippocampal regions. Scale bars = 200 μ m in A–D.

ing interneurons have been described (Ribak et al., 1985; Frotscher et al., 1991; Gulyas et al., 1992; Soriano and Frotscher, 1994). Thus, our data indicate that spine-bearing principal cells and a subset of interneurons synthesize Synaptopodin in the mouse hippocampus.

Quantification of regional *synaptopodin* mRNA expression

To determine whether region-specific differences in the number of Synaptopodin-positive puncta could be caused by different levels of *synaptopodin* mRNA expression,

quantitative RT-PCR was performed. Because the majority of neurons expressing *synaptopodin* in the hippocampus are located in the granule cell layer of the dentate gyrus and the pyramidal layers of areas CA3 and CA1, portions of these cell layers were selectively cut from toluidine blue stained brain sections by laser microdissection (Fig. 6B–D). Total RNA was extracted, reverse transcribed and then subjected to real-time PCR to quantify the amount of *synaptopodin* mRNA in each sampled tissue. To compare *synaptopodin* mRNA expression in the dentate gyrus and the hippocampal subfields, the *synaptopodin* mRNA level in the granule cell layer of the dentate gyrus was used as a reference point for relative quantification. Compared with expression levels in the granule cell layer, *synaptopodin* mRNA levels in CA1 and CA3 areas did not reveal any statistically significant differences (Fig. 6E). Relative expression levels were 1.07 ± 0.7 (mean \pm SD) in area CA3 and 1.52 ± 0.73 in area CA1.

DISCUSSION

Synaptopodin is an actin-associated molecule essential for the spine apparatus organelle (Deller et al., 2003). Because Synaptopodin and the spine apparatus are believed to play an important role in synaptic plasticity, it is of interest to know more about their normal distribution in the brain. The present study extends our previous reports on the region and lamina-specific distribution of Synaptopodin in the mouse hippocampus and demonstrates that a lamina-specific distribution of Synaptopodin is also found within dendritic segments of identified hippocampal principal neurons. In addition, the present data demonstrate that Synaptopodin-positive puncta are primarily located in spines, where they are bona fide indicators of the spine apparatus organelle. We conclude, on the basis of the Synaptopodin distribution pattern, that the spine apparatus organelle is distributed in a region- and layer-specific manner in the mouse hippocampus.

Regional and laminar variations of Synaptopodin are not caused by partial presynaptic localization of Synaptopodin protein or regional variations in *synaptopodin* mRNA expression

In our previous analyses of Synaptopodin in the rodent hippocampus, we were struck by its nonhomogeneous immunostaining pattern (Deller et al., 2000a, 2002), which corresponded to the laminar organization of the hippocampus generated by the layer-specific termination of afferent fiber systems (Amaral and Witter, 1995). This pattern was intriguing, because Synaptopodin, which is believed to be a postsynaptic molecule, follows a pattern generated by presynaptic structures. This finding suggested that Synaptopodin is differentially distributed along dendrites in response to presynaptic signals (Deller et al., 2002). Although such a hypothesis is plausible, direct proof for the differential distribution of Synaptopodin along hippocampal principal cell dendrites has yet to be provided and other explanations, such as a partial presynaptic localization of Synaptopodin need to be firmly excluded.

In our previous study, we have analyzed the subcellular distribution of Synaptopodin at the ultrastructural level using pre- and postembedding immunogold techniques

(Deller et al., 2000a, 2002). Although we did not observe a presynaptic localization of Synaptopodin in this analysis, a partial localization of Synaptopodin on afferent terminals in some hippocampal layers may have escaped detection in these high-resolution studies. Thus double-immunofluorescence for Synaptophysin and Synaptopodin was used in the present study, which made it possible to analyze a large number of pre- and postsynaptic structures in the various regions and layers of the hippocampus. Because we did not observe a single case of colocalization of Synaptopodin with Synaptophysin, we conclude with confidence, that Synaptopodin is not located on presynaptic afferent terminals in the hippocampus. Thus, the laminar immunostaining pattern of Synaptopodin is not caused by a partial presynaptic localization of this molecule.

As far as the regional differences in Synaptopodin immunostaining are concerned, for example, between the dentate gyrus and area CA1, these could also be caused by regional differences in the cellular *synaptopodin* mRNA levels. To measure regional *synaptopodin* mRNA levels, hippocampal principal cells were microdissected using the laser capture microdissection technique and cellular *synaptopodin* mRNA expression levels were measured using quantitative RT-PCR (Burbach et al., 2003). Even with this very-sensitive quantitative approach no significant differences in *synaptopodin* mRNA levels were observed between the different principal cell populations of the hippocampus. Thus, we conclude that regional differences in Synaptopodin-immunostaining are not caused by regional differences in *synaptopodin* mRNA levels.

Laminar variations of Synaptopodin-immunostaining are caused by the lamina-specific distribution of Synaptopodin in hippocampal principal neurons

To provide positive proof for a lamina-specific distribution of Synaptopodin at the cellular level, dendritic segments of EGFP-labeled hippocampal neurons were stained for Synaptopodin and analyzed in the various hippocampal layers. In agreement with the hypothesis that Synaptopodin is differentially sorted along dendrites, significant differences in the percentage of Synaptopodin-positive spines were found between the layers (Fig. 4E). In some regions, such as area CA1, these differences were almost 2.3-fold between different dendritic segments of the same cell type. Thus, a lamina-specific distribution of Synaptopodin is present at the cellular level.

After demonstrating the layer-specific distribution of Synaptopodin within identified principal cell dendrites, we wondered whether this distribution could also explain the distribution of Synaptopodin at the tissue level. Because Synaptopodin tissue densities can be calculated by multiplying the layer-specific percentage of Synaptopodin-positive spines with the layer-specific density of spines, we calculated tissue densities on the basis of our cellular data and compared these results with our density measurements. If the results were similar, this would indicate that the layer-specific distribution of Synaptopodin in the hippocampus is caused by the layer-specific distribution of Synaptopodin within principal cells. The dentate gyrus shall serve as an example for this approach: In the present study, the layer-specific percentage of Synaptopodin-positive spines/dendritic segment was determined in the

inner (28.6%) and the outer molecular layer (36.6%) of the dentate gyrus. Synapse densities—which can roughly be equated to spine densities in the molecular layer of the dentate gyrus—have been published previously (inner molecular layer, 30/100 μm^2 ; outer molecular layer, 35/100 μm^2 ; Matthews et al., 1976; Hoff et al., 1981). These data were used to calculate Synaptopodin densities for the inner molecular layer (8.58 positive spines/100 μm^2), the outer molecular layer (12.81 positive spines/100 μm^2), and the ratio between the two layers (outer molecular layer/inner molecular layer = 1.49). This ratio was compared with the ratio between the outer and inner molecular layer obtained from the density measurements (outer molecular layer, 214.6 puncta/1,000 μm^3 ; inner molecular layer, 147.2 puncta/1,000 μm^3 ; outer molecular layer/inner molecular layer = 1.46). Because these two ratios are very close, we conclude that the cellular data can be converted into puncta densities, if layer-specific spine densities are taken into account. Thus, the layer-specific distribution of Synaptopodin within single cells sufficiently explains the layer-specific distribution of Synaptopodin at the tissue level.

Synaptopodin labels the spine apparatus organelle in spines of hippocampal principal neurons

Although Synaptopodin has been recognized previously as a molecule that is essential for the formation of a spine apparatus (Deller et al., 2003), some doubts have remained whether or not Synaptopodin is a fairly specific marker for this organelle. For example, the detection of Synaptopodin-positive material in dendrites (Deller et al., 2000a) raised the question whether Synaptopodin could also be located to a large extent in dendritic shafts. We addressed this issue in the present study and quantified the number of Synaptopodin-positive puncta in spines and dendritic shafts in the different hippocampal layers. Our data show that the overwhelming majority (>95%; exception, *stratum lacunosum-moleculare* of CA1) of Synaptopodin-positive puncta are located in spines. The size and location of these puncta correspond to the size and location of the spine apparatus organelle, as it has been documented and described in detail by others (Gray, 1959; Spacek, 1985; Spacek and Harris, 1997). Moreover, the percentage of Synaptopodin-positive puncta determined in *stratum radiatum* of CA1 nicely corresponds to the percentage of spine apparatus bearing spines determined by three-dimensional electron microscopic reconstruction in this layer in the rat (Spacek and Harris, 1997). Taking our own ultrastructural investigations into account, in which we showed that Synaptopodin immunoreactivity in spines is associated with a spine apparatus (Deller et al., 2000a), we conclude that more than 95% of all Synaptopodin puncta in dendrites represent Synaptopodin-positive spine apparatuses. Thus, Synaptopodin appears to be a highly specific and useful marker for labeling the spine apparatus organelle in the hippocampus.

Distribution of the spine apparatus in the mouse hippocampus is region- and lamina-specific

Because the overwhelming majority of Synaptopodin-puncta represent spine apparatuses, we conclude from our

data that this intriguing organelle shows a region- and lamina-specific distribution in the hippocampus. In mice, it appears to be most abundant in spines of dentate granule cells located in the middle molecular layer and relatively scarce in spines of CA1 pyramidal neurons located in *stratum oriens*. This differential distribution of the spine apparatus may be of functional importance, because this organelle has been assumed to be a calcium store (Fifkova et al., 1983; Lisman, 1989; Svoboda and Mainen, 1999), which is probably involved in calcium-dependent changes in synaptic plasticity (Miyata et al., 2000; Sabatini et al., 2002). In line with this interpretation, mice lacking the spine apparatus organelle showed deficits in long-term potentiation and impairment in learning and memory tests (Deller et al., 2003). It will now be of considerable interest to find out whether or not the presence of a spine apparatus influences Ca^{2+} -transients or synaptic plasticity of individual spines. The normal distribution of Synaptopodin in identified hippocampal neurons is, however, an important baseline for this future work.

Synaptic activity of afferent fiber systems may regulate lamina-specific sorting of Synaptopodin

After documenting intracellular sorting of Synaptopodin and the spine apparatus in hippocampal principal cells, it is now of interest to understand the cellular processes that are involved. Although nothing is known about the molecular machinery that is required for the intracellular sorting of Synaptopodin, several data sets provide insights into the signals that may regulate the lamina-specific distribution of this molecule. These data suggest that sorting of Synaptopodin occurs in response to signals provided by afferent fibers, most likely in response to their synaptic activity: First, the lamina-specific distribution of Synaptopodin in normal mice and its loss in reeler mice indicate that the laminar fiber- and cytoarchitecture of the hippocampus underlies the distribution of Synaptopodin-positive puncta (Deller et al., 2002). If the laminar organization of afferent fibers is disrupted, lamina-specific sorting does not occur. Second, Synaptopodin labels the spine apparatus, which consists of sacs of smooth endoplasmic reticulum interdigitated by electron-dense material (Gray, 1959; Spacek, 1985). Because smooth endoplasmic reticulum can be recruited to the spine or added to the spine apparatus in an activity-dependent manner (Tarrant and Routtenberg, 1979; Spacek and Harris, 1997; Halpain, 2000; Capani et al., 2001), changes in synaptic activity are likely to regulate the inclusion or construction of Synaptopodin-positive spine apparatuses in spines. Third, and most importantly, changes in hippocampal synaptic activity, for example, after kainic acid injection (Roth et al., 2001) or the induction of hippocampal long-term potentiation in vivo (Yamazaki et al., 2001; Fukazawa et al., 2003), lead to lamina-specific alterations in the distribution of Synaptopodin-protein in the hippocampus. Taken together, these data provide strong evidence for an activity-dependent sorting of Synaptopodin. On the basis of these and our data, we would like to suggest the following hypothetical model: *Synaptopodin* mRNA is expressed at basal levels in hippocampal principal neurons, translated into Synaptopodin protein in the cell soma, and transported to the spine compartment by a yet unknown molecular mechanism. Targeting to specific spines would

then be achieved by local signals following activation of a specific axospinous synapse. Within these spines, Synaptopodin—an essential component of the spine apparatus—could then either enlarge an existing spine apparatus or participate in the de novo construction of this organelle.

ACKNOWLEDGMENTS

The authors thank Dr. Estifanos Ghebremedhin for help with statistical analysis and Dr. Michael Calhoun for comments on the article. Daniela Brückner, Ute Fertig, Markus Haubner, Barbara Nagel, and Charlotte Nolte-Uhl contributed to this study by providing excellent technical assistance.

LITERATURE CITED

- Amaral DG, Witter MP. 1995. In: Paxinos G, editor. The rat nervous system. San Diego: Academic Press. p 443–494.
- Burbach GJ, Dehn D, Del Turco D, Deller T. 2003. Quantification of layer-specific gene expression in the hippocampus: effective use of laser microdissection in combination with quantitative RT-PCR. *J Neurosci Methods* 131:83–91.
- Capani F, Martone ME, Deerinck TJ, Ellisman MH. 2001. Selective localization of high concentrations of F-actin in subpopulations of dendritic spines in rat central nervous system: a three-dimensional electron microscopic study. *J Comp Neurol* 435:156–170.
- Deller T, Merten T, Roth SU, Mundel P, Frotscher M. 2000a. Actin-associated protein synaptopodin in the rat hippocampal formation: localization in the spine neck and close association with the spine apparatus of principal neurons. *J Comp Neurol* 418:164–181.
- Deller T, Mundel P, Frotscher M. 2000b. Potential role of synaptopodin in spine motility by coupling actin to the spine apparatus. *Hippocampus* 10:569–581.
- Deller T, Haas CA, Deissenrieder K, Del Turco D, Coulin C, Gebhardt C, Drakew A, Schwarz K, Mundel P, Frotscher M. 2002. Laminar distribution of synaptopodin in normal and reeler mouse brain depends on the position of spine-bearing neurons. *J Comp Neurol* 453:33–44.
- Deller T, Korte M, Chabanis S, Drakew A, Schwegler H, Stefani GG, Zuniga A, Schwarz K, Bonhoeffer T, Zeller R, Frotscher M, Mundel P. 2003. Synaptopodin-deficient mice lack a spine apparatus and show deficits in synaptic plasticity. *Proc Natl Acad Sci U S A* 100:10494–10499.
- Feng G, Mellor RH, Bernstein M, Keller-Peck C, Nguyen QT, Wallace M, Nerbonne JM, Lichtmann JW, Sanes JR. 2000. Imaging neuronal subsets in transgenic mice expressing multiple spectral variants of GFP. *Neuron* 28:41–51.
- Fifkova E, Markham JA, Delay RJ. 1983. Calcium in the spine apparatus of dendritic spines in the dentate molecular layer. *Brain Res* 266:163–168.
- Frotscher M, Seress L, Schwerdtfeger WK, Buhl E. 1991. The mossy cells of the fascia dentata: a comparative study of their fine structure and synaptic connections in rodents and primates. *J Comp Neurol* 312:145–163.
- Fukazawa Y, Saitoh Y, Ozawa F, Ohta Y, Mizuno K, Inokuchi K. 2003. Hippocampal LTP is accompanied by enhanced F-actin content within the dendritic spine that is essential for late LTP maintenance in vivo. *Neuron* 38:447–460.
- Gray EG. 1959. Axo-somatic and axo-dendritic synapses of the cerebral cortex: an electron microscopic study. *J Anat* 83:420–433.
- Gulyas AI, Miettinen R, Jacobowitz DM, Freund TF. 1992. Calretinin is present in non-pyramidal cells of the rat hippocampus: I. A new type of neuron specifically associated with the mossy fibre system. *Neuroscience* 48:1–27.
- Halpain S. 2000. Actin and the agile spine: how and why do dendritic spines dance? *Trends Neurosci* 23:141–146.
- Hamlyn LH. 1962. The fine structure of the mossy fibre endings in the hippocampus of the rabbit. *J Anat* 97:112–120.
- Hoff SF, Scheff SW, Kwan AY, Cotman CW. 1981. A new type of lesion-induced synaptogenesis: I. synaptic turnover in non-denervated zones of the dentate gyrus in young adult rats. *Brain Res* 222:1–13.
- Lisman J. 1989. A mechanism for the Hebb and anti-Hebb processes underlying learning and memory. *Proc Natl Acad Sci U S A* 86:9574–9578.
- Matthews DA, Cotman CW, Lynch G. 1976. An electron microscopic study of lesion-induced synaptogenesis in the dentate gyrus of the adult rat. I. Magnitude and time course of degeneration. *Brain Res* 115:1–21.
- Miyata M, Finch EA, Khirouq L, Hashimoto K, Hayasaka S, Oda SI, Inouye M, Takagishi Y, Augustine GJ, Kano M. 2000. Local calcium release in dendritic spines required for long-term synaptic depression. *Neuron* 28:233–244.
- Mundel P, Heid HW, Mundel TM, Kruger M, Reiser J, Kriz W. 1997. Synaptopodin: an actin-associated protein in telencephalic dendrites and renal podocytes. *J Cell Biol* 139:193–204.
- Ribak CE, Seress L, Amaral DG. 1985. The development, ultrastructure and synaptic connections of the mossy cells of the dentate gyrus. *J Neurocytol* 14:835–857.
- Roth SU, Sommer C, Mundel P, Kiessling M. 2001. Expression of synaptopodin, an actin-associated protein, in the rat hippocampus after limbic epilepsy. *Brain Pathol* 11:169–181.
- Sabatini BL, Oertner TG, Svoboda K. 2002. The life cycle of Ca²⁺ ions in dendritic spines. *Neuron* 33:439–452.
- Soriano E, Frotscher M. 1994. Mossy cells of the rat fascia dentata are glutamate-immunoreactive. *Hippocampus* 4:65–70.
- Spacek J. 1985. Three-dimensional analysis of dendritic spines. II. Spine apparatus and other cytoplasmic components. *Anat Embryol (Berl)* 171:235–243.
- Spacek J, Harris KM. 1997. Three-dimensional organization of smooth endoplasmic reticulum in hippocampal CA1 dendrites and dendritic spines of the immature and mature rat. *J Neurosci* 17:190–203.
- Svoboda K, Mainen ZF. 1999. Synaptic [Ca²⁺]: intracellular stores spill their guts. *Neuron* 22:427–430.
- Tarrant SB, Routtenberg A. 1979. Postsynaptic membrane and spine apparatus: proximity in dendritic spines. *Neurosci Lett* 11:289–294.
- Weins A, Schwarz K, Faul C, Barisoni L, Linke WA, Mundel P. 2001. Differentiation- and stress-dependent nuclear cytoplasmic redistribution of myopodin, a novel actin-bundling protein. *J Cell Biol* 155:393–404.
- Yamazaki M, Matsuo R, Fukazawa Y, Ozawa F, Inokuchi K. 2001. Regulated expression of an actin-associated protein, synaptopodin, during long-term potentiation. *J Neurochem* 79:192–199.